The Astrophysical Journal Supplement Series, 151:387–397, 2004 April

A MEDIUM-RESOLUTION NEAR-INFRARED SPECTRAL LIBRARY OF LATE-TYPE STARS. I.

Valentin D. Ivanov
European Southern Observatory, Karl-Schwarzschild-Strasse 2, D-85748 Garching bei München, Germany; vivanov@eso.org

Marcia J. Rieke, Charles W. Engelbracht, Almudena Alonso-Herrero,[1] and George H. Rieke
Steward Observatory, University of Arizona, Tucson, AZ 85721; mrieke@as.arizona.edu, chad@as.arizona.edu, grieke@as.arizona.edu, aalonso@as.arizona.edu

and

Kevin L. Luhman
Harvard-Smithsonian Center for Astrophysics, 60 Garden Street, Cambridge, MA 02138; kluhman@cfa.harvard.edu
Received 2003 March 13; accepted 2003 December 2

ABSTRACT

We present an empirical infrared spectral library of medium-resolution ($R \approx 2000-3000$) H (1.6 μm) and K (2.2 μm) band spectra of 218 red stars, spanning a range of [Fe/H] from ~-2.2 to $\sim+0.3$. The sample includes Galactic disk stars, bulge stars from Baade's window, and red giants from Galactic globular clusters. We report the values of 19 indices covering 12 spectral features measured from the spectra in the library. Finally, we derive calibrations to estimate the effective temperature, and diagnostic relationships to determine the luminosity classes of individual stars from near-infrared spectra.

This paper is part of a larger effort aimed at building a near-IR spectral library to be incorporated in population synthesis models, as well as at testing synthetic stellar spectra.

Subject headings: atlases — infrared: stars — stars: abundances — stars: chromospheres — stars: fundamental parameters — stars: late-type

On-line material: machine-readable tables

1. INTRODUCTION

Over the last two decades, evolutionary synthesis modeling has become a common tool to study unresolved stellar populations of galaxies in the optical and UV passbands (Bruzual & Charlot 1993; Worthey 1994; Vazdekis 1999; Leitherer et al. 1999). The heavy obscuration in starburst galaxies—often with $A_V \geq 5$ mag (Engelbracht 1997)—requires an expansion of these models into the near-infrared (IR) domain, because the extinction there is reduced tenfold in comparison with the optical region: $A_K/A_V = 0.112$ (Rieke & Lebofsky 1985). Therefore, it is not surprising that many studies of embedded stellar populations in galaxies have been conducted in the near-IR (Rieke et al. 1980, 1993).

IR evolutionary synthesis models based on synthetic spectra (Origlia, Moorwood, & Oliva 1993; Kurucz 1994) generally have difficulties reproducing broadband colors because of the complicated opacity calculations in the near-IR. Empirical libraries based predominantly on bright and nearby Milky Way stars (Kleinmann & Hall 1986; Lançon & Rocca-Volmerange 1992; Wallace & Hinkle 1996, 1997; Meyer et al. 1998; Wallace et al. 2000) are limited to near solar metallicity. At the same time, realistic galaxy modeling requires metallicities ranging from [Fe/H] $= -1.76$ for the most metal-poor galaxy known, I Zw 18 (Aloisi et al. 2003), to supersolar values, measured for at least for some giant elliptical galaxies (Casuso et al. 1996).

The properties of the most prominent near-IR spectral libraries available in the literature are summarized in Table 1. For a review of the earlier work see Merril & Ridgway (1979). This summary shows that despite the sizable quantity of available stellar spectra, up until now there was no uniform near-IR data set with high signal-to-noise ratio and resolution, covering the entire range of spectral classes, luminosity, and metallicity necessary to carry out evolutionary population synthesis in the near-IR. The deficit of some types of stars such as metal-poor super giants is understandable in the context of the Milky Way star formation history, but the lack of many other types is rectifiable. We concentrate on metal features that have equivalent widths in a typical starburst galaxy larger than 1 Å—as they can be measured reliably in spectra with signal-to-noise ratios of $\sim$30–50 (Engelbracht 1997).

A second application of our library, albeit no less important, is the analysis of individual stars hidden behind $A_V \geq 10$ mag of visual extinction. A typical case for such a population is represented by the Arches cluster members.

Here we describe the observations and the sample of an empirical near-IR stellar library that is designed to meet the requirements of population synthesis. The main advantage in comparison with previous work is the expanded metallicity coverage. We also present a few diagnostics methods to derive parameters of individual stars. The evolutionary population model will be published in a subsequent paper. The next section describes the observations and the data reduction technique. Section 3 summarizes the sample selection. Spectral indices are defined in § 4, and some diagnostic applications for parameters of individual stars are considered in § 5. In § 6, we give the summary.

2. OBSERVATIONS AND DATA REDUCTION

The near-IR spectra were taken from 1995 to 1999 mainly at the Steward Observatory 2.3 m Bok telescope on Kitt Peak. Some stars were observed at the original 4.5 m MMT and at the Steward Observatory 1.55 m Kuiper telescope. We used FSpec

[1] Present address: Departamento de Astrofísica Molecular e Infrarroja, IEM, Consejo Superior de Investigaciones Científicas, Serrano 113b, 28006 Madrid, Spain.

TABLE 1
NEAR-IR SPECTRAL LIBRARIES

Spectral Library Reference	λ (μm)	Spectral Type and Luminosity Class Range	Number of Stars	Spectral Resolution
Johnson & Mèndez 1970	1.2–2.5	A–M, I–V	32	550
Kleinmann & Hall 1986	2.0–2.5	F–M, I–V	26	2500–3100
Lançon & Rocca–Volmerange 1992	1.4–2.5	O–M, I–V	56	550
Origlia et al. 1993	1.5–1.7	G–M, I–V	40	1500
Ali et al. 1995	2.0–2.4	F–M, V	33	1380
Wallace & Hinkle 1996	2.02–2.41	G–M, I–V	12	45000
Dallier et al. 1996	1.57–1.64	O–M, I–V	37	1500–2000
Hanson et al. 1996	2.0–2.4	O–B, I–V	180	800–3000
Ramírez et al. 1997	2.19–2.34	K–M, III	43	1380, 4830
Wallace & Hinkle 1997	2.0–2.4	O–M, I–V	115	3000
Meyer et al. 1998	1.5–1.7	O–M, I–V	85	3000
Joyce 1998	1.0–2.5	K–M, III	29	500–1500
Förster-Schreiber 2000	1.90–2.45	G–M, I–III	31	830,3000
Wallace et al. 2000	1.05–1.34	O–M, I–V	88	3000
Lançon & Wood 2000	0.5–2.5	K–M, I–III	77	1100
Hicks et al. 2000	1.08–1.35	O–M, I–V	105	650
This work	1.48–2.45	G–M, I–V	218	2000–3000

NOTE.—This work is included for comparison.

(Williams et al. 1993), a cryogenic long-slit near-IR spectrometer utilizing a NICMOS3 256×256 array (Kozlowski et al. 1993). The majority of the stars were observed with a 600 line mm^{-1} grating, corresponding to a spectral resolution $R \approx 2000$–3000. This is the highest useful spectral resolution for studies of stellar populations in external galaxies where the intrinsic velocity dispersion smooths out the integrated spectra. The rest were observed with a 300 line mm^{-1} grating and $R \approx 1000$–1500. The slit widths were 2.″4 at the 2.3 m telescope, 1.″2 at the MMT, and 3.″6 at the 1.55 m telescope. The plate scales were 1.2, 0.6, and 1.8 arcsec pixel^{-1}, respectively. The limited physical size of the near-IR array required the acquisition of spectra at 10–12 grating positions, corresponding to different central wavelengths (λ_c) to cover the entire H and K atmospheric windows with sufficient overlap. Usually, one of the following two combinations of λ_c was used: 1.54, 1.62, 1.70, 2.06, 2.13, 2.19, 2.245, 2,31, 2.37, 2.42 μm, or 1.50, 1.57, 1.64, 1.71, 2.05, 2.10, 2.15, 2.20, 2.25, 2.30, 2.35, 2.40 μm. The log of observations is given in Table 2.

The observing strategy for a single setting included nodding the telescope to obtain spectra at four (at the MMT) or six (at the 2.3 m and 1.55 m telescopes) different positions along the slit, and integrating at each position for 3–20 s, depending on the apparent brightness of the object and the sky background. This was necessary in order to (*i*) carry out the sky emission subtraction and account for the sky background variations by

TABLE 2
LOG OF SPECTROSCOPIC OBSERVATIONS

Date (1)	Site (2)	Star (3)	Standard (4)	Spectral Type (5)	Grating (6)	Range (7)
951209	61	S074439	S074506	A3 V	600	*HK*
951209	61	S060890	HR 3348	A0 V	600	*HK*
951209	61	S027179	HR 3592	A2 V	600	*HK*
951209	61	VY Leo	HR 4244	A3 V	600	*H*
951210	61	S074175	HR 0277	A2 V	600	*HK*
951210	61	S109474	HR 0081	A0 V	600	*HK*
951210	61	S109471	HR 0081	A0 V	600	*HK*
951210	61	S074883	HR 0669	A1 V	600	2.30–2.40
951210	61	S080333	HR 3481	A1 V	600	*HK*
951210	61	S098021	HR 3481	A1 V	600	*HK*

NOTES.—Table 2 is available in its entirety in the electronic edition of the *Astrophysical Journal Supplement*. A portion is shown here for guidance regarding its form and content. (Col. [1]) Date of the observation, in yymmdd format, e.g., 990203 is the night of 1999 February 3–4. (Col. [2]) Sites: 61, 90, MM—Steward Observatory 1.55 m, 2.3 m, and the original MMT telescopes, respectively. (Col. [3]) Object: S = SAO, H = HD, N = NGC, B = BD. (Col. [4]) Standard star for the atmospheric correction. (Col. [5]) Spectral type for the standard star. (Col. [6]) Gratings: 600 lines mm^{-1} corresponds to spectral resolution $R \approx 3000$, and 300 lines mm^{-1} corresponds to $R \approx 1500$. (Col. [7]) Spectral range covered: H and K indicate that the entire atmospheric window was observed. Numbers give the central wavelength of the observed grating settings in μm. Two numbers separated by a dash means that all grating settings in between them were observed. A number in parentheses after H and/or K with a minus indicates a missing setting.

having a sky taken just before and after the science exposures; and (*ii*) improve the pixel sampling, flat-fielding, and bad pixel correction by having the object placed on multiple positions on the array.

Next, we repeated the same procedure for a standard star at similar air mass (air mass difference $\leq$0.1–0.15) to correct for the atmospheric absorption. Then we changed the grating setting, obtained a sequence of 4–6 spectra of the standard, moved the telescope back to the object, and repeated the same procedure at the new grating setting. Occasionally, if two or three target stars were available nearby on the sky, we increased the observing efficiency by using the same telluric standard for all of them.

The spectra were reduced using IRAF[2] tasks written specifically for FSpec. An average of the sky backgrounds taken immediately before and after each object was subtracted to remove simultaneously the sky emission lines, and the dark current and bias level. Dark-subtracted illuminated dome flats taken at the same central wavelengths as the science exposures were applied to correct for pixel-to-pixel variations. The known bad pixels were masked out. Object images were shifted (using centroid fitting across the continuum) and median combined to produce a single two-dimensional spectrum. The large number of object images allowed us to reject any remaining bad pixels and cosmic rays. One-dimensional spectra were extracted by fitting a polynomial of order 3–5 to the continuum in the two-dimensional image with the IRAF task "apall." The spatial width of the extraction apertures was usually 3–5 pixels, depending on the scale and the seeing.

In most cases the object spectra were divided by spectra of solar analog stars observed at the same air mass and then multiplied by the solar spectrum (Livingston & Wallace 1991) to remove the effects of the photospheric absorption (Maiolino, Rieke, & Rieke 1996). The standard stars were not always exactly G2 dwarfs (usually ranging from F8 V to G3 V), and the true shape of the continuum had to be restored by multiplying the spectra by the ratio of blackbodies with the standard star and solar effective temperatures. In the cases we chose nearby A stars for telluric standards as an alternative of the solar analogs, we multiplied by another A star spectrum, already corrected for the photospheric absorption with a G2 V star. If an A type standard was used to correct only a *K*-band spectrum, we removed the Brγ feature by interactively fitting and subtracting a Gaussian with the task " splot." We carried out the wavelength calibration using OH airglow lines (Oliva & Origlia 1992) complemented if necessary with Ne–Kr lamp spectra.

The spectrum at each individual setting was divided by second- or third-order polynomial continuum fits and combined with the rest of the settings to construct a single *HK* spectrum. Finally, we multiplied the spectrum by a blackbody with stellar effective temperature corresponding to the spectral type (Schmidt-Kaler 1982; Straižys 1992). Unfortunately, the normalization procedure removes the broad vapor absorption features in the coolest stars, but this loss is unavoidable because the spectral extent of a single setting is only 0.075–0.095 μm and does not provide sufficient coverage for a reliable estimate of the continuum shape. Furthermore, in many cases the true continuum shape was distorted by the imperfect spectral type match of the telluric standards, as discussed above. The deviation between the constructed continuum shape and the real one is most severe for late M stars, where the molecular absorption is the strongest. A possible way to alleviate this problem completely is to impose on our spectra empirical continuum shapes taken from lower resolution spectra (Lançon & Rocca-Volmerange 1992; Lançon & Wood 2000). We intend to explore this avenue in the future.

The error analysis of spectra that consist of "pieces" taken at different times, and often on different nights, is particularly complicated because of the large variations of the signal-to-noise ratio (S/N) across the individual spectra. The uncertainties are dominated by systematic errors due to (*i*) sky emission and transparency variations with wavelength and (*ii*) temporal changes in the observing conditions. An example is given in Figure 1, where the difference between the "final" spectra of two different K3 III stars with near solar metallicity is shown. The difference Δ has been divided by the average of the two spectra. The inset shows the distribution of these differences. Their average difference $\langle\Delta\rangle$ is statistically indistinguishable from zero, and the value of the standard deviation σ suggests that each spectrum has an average $S/N \sim 50$. At the same time, the photon statistics suggests $S/N \sim 150$. The inconsistency is largely due to the variation of the sky background and transmission. Therefore, a single signal-to-noise ratio does not represent well the quality of the data. Furthermore, the measurements of individual features of interest include additional systematic uncertainties, such as the continuum placement during the continuum normalization, and differences between the stars used for the telluric correction and the Sun.

The best technique to estimate the actual signal-to-noise ratio is to measure the noise locally over a "clean" continuum region near the spectral feature of interest. We recommend this method for applications concerning parameters of individual

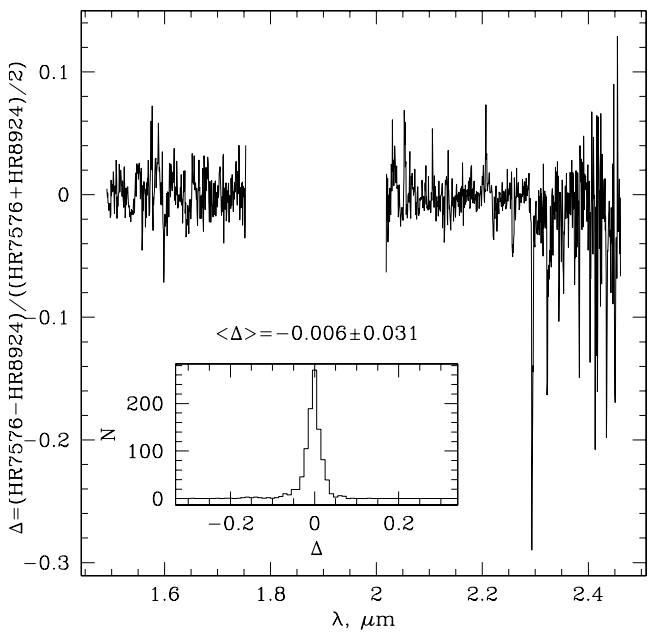

FIG. 1.—Data quality: difference Δ between the spectra of two K3 III stars—HR 7576 and HR 8924—with similar abundances, normalized by the average of the two spectra as a function of wavelength (in arbitrary flux units). The inset shows the histogram of the differences. The means and the standard deviation of the distribution are also shown.

[2] IRAF is distributed by the National Optical Astronomy Observatories, which are operated by the Association of Universities for Research in Astronomy, Inc., under cooperative agreement with the National Science Foundation.

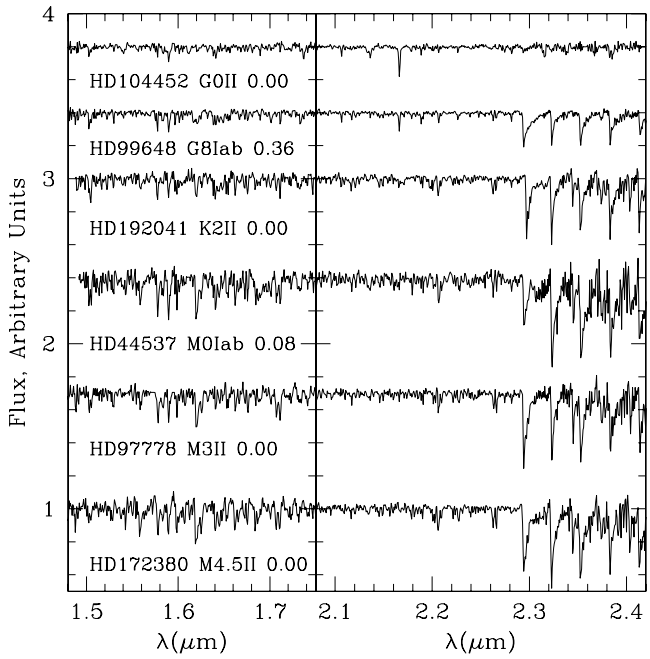

FIG. 2.—Subset of *H* and *K* spectra of supergiants. The names of the stars, spectral types, and [Fe/H] are indicated. The spectra are continuum divided and shifted vertically for display purposes by adding (*from bottom to top*) 0.0, 0.7, 1.4, 2.0, 2.4, and 2.8.

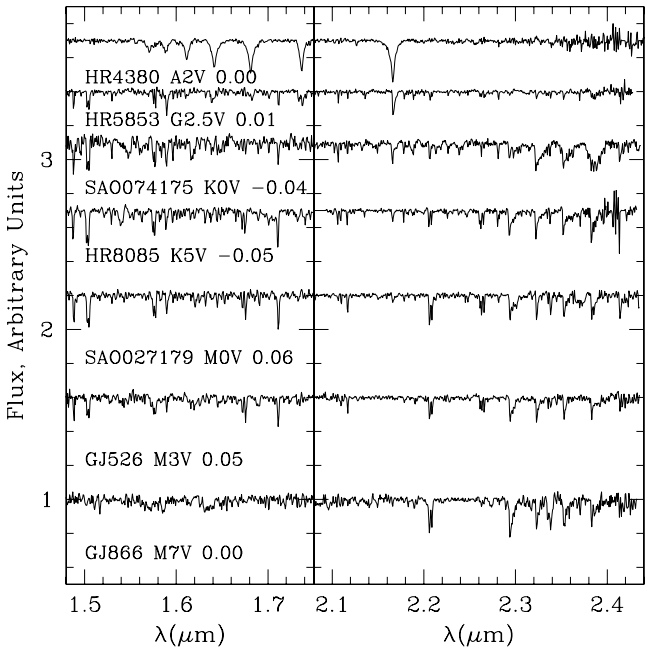

FIG. 4.—Subset of *H* and *K* spectra of main-sequence stars. The names of the stars, spectral types, and [Fe/H] are indicated. The spectra are continuum divided and shifted vertically for display purposes by adding (*from bottom to top*) 0.0, 0.6, 1.2, 1.7, 2.1, 2.4, and 2.7.

stars. Our study shows that for statistical work the uncertainties of indices can be approximated as $\sigma(\text{Index}) = 0.2 \times \text{Index}$, with a lower limit of $\sigma(\text{Index}) = 0.02$ mag. Representative subsets of our spectra are shown in Figures 2, 3, 4, and 5.

3. SAMPLE SELECTION AND STELLAR PARAMETERS

We have assembled an IR spectral library of 218 stars. The majority of them have photospheric parameters available from the literature. The main criterion to include various types of stars was to populate the *effective temperature–surface gravity–abundance* space necessary to model the stellar populations of starburst galaxies. Special attention was paid to observing red supergiants, which dominate the near-IR flux of these galaxies.

The largest fraction of stars in our library was selected from the Lick group sample (Worthey et al. 1994), assuring that they have high-quality optical spectra and known spectral type, surface gravity, and metallicity. However, the Lick library was

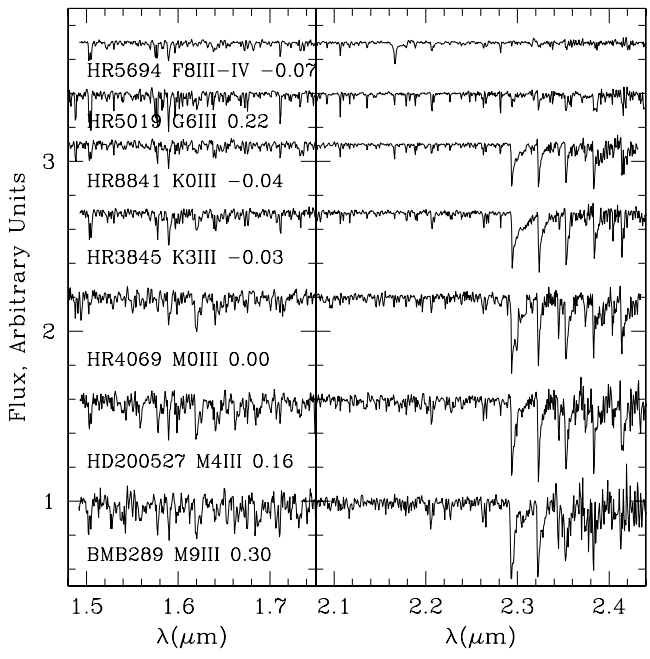

FIG. 3.—Subset of *H* and *K* spectra of giants. The names of the stars, spectral types, and [Fe/H] are indicated. The spectra are continuum divided and shifted vertically for display purposes by adding (*from bottom to top*) 0.0, 0.6, 1.2, 1.7, 2.1, 2.4, and 2.7.

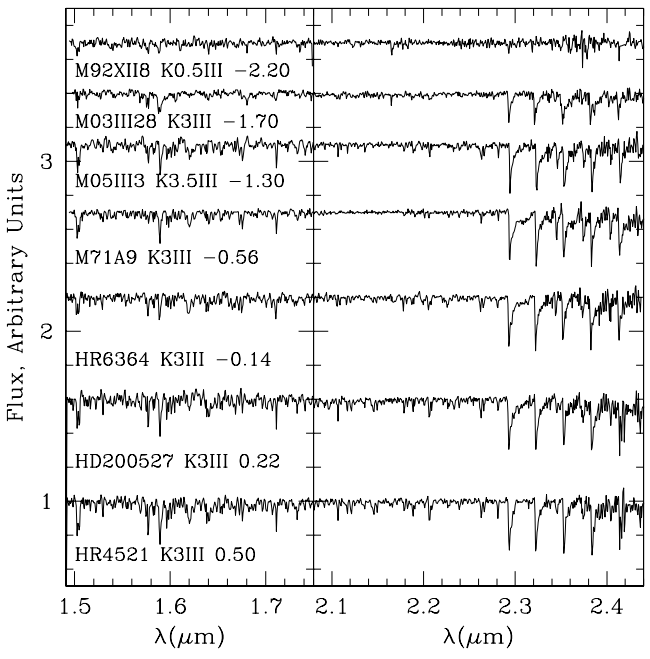

FIG. 5.—Subset of *H* and *K* spectra for a selection of K giants spanning a range of metallicities. The names of the stars, spectral types, and [Fe/H] are indicated. The spectra are continuum divided and shifted vertically for display purposes by adding (*from bottom to top*) 0.0, 0.6, 1.2, 1.7, 2.1, 2.4, and 2.7.

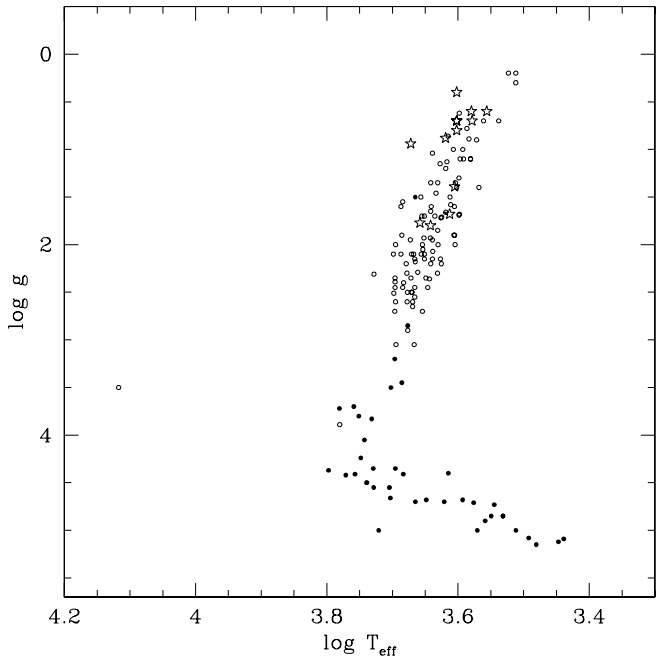

FIG. 6.—Content of the library: distribution of the library stars on the surface gravity log g vs. effective temperature $T_{\rm eff}$ plane. Star symbols are supergiants, circles are giants, and solid dots are subgiants and dwarfs. The "anomalous" subgiant at log $g = 1.5$ is extremely metal-poor, with [Fe/H] $= -2.67$.

aimed at modeling galaxies with old stellar populations—ellipticals and bulges of spirals—and therefore, is mainly composed of giants and dwarfs. We observed most red giants from their sample, and supplemented this set with super–metal-rich stars from the Baade's Window region from McWilliam & Rich (1994) to expand their metallicity range. Next, we selected red supergiant stars from White & Wing (1978) and Luck & Bond (1989), to assure good coverage of the stars that dominate the stellar populations of galaxies with ages of 7–12 Myr—the so-called red-supergiant-phase. In addition, we observed various stars with known metal abundances from the catalog of Cayrel de Strobel et al. (1997). The distribution of our stars on the surface gravity log g versus effective temperature $T_{\rm eff}$ relation is shown in Figure 6.

The photospheric data for the program stars are summarized in Table 3. About half of them (111 out of 218 stellar metallicities) were already available from Faber et al. (1985), Gorgas et al. (1993), and Worthey et al. (1994). The last work offers recalculated stellar parameters based on their own spectral line measurements and calibrations. To ensure that our system is as close as possible to theirs, we used these new estimates when available. In addition, we carried out an extensive literature search for photospheric data for the rest of our program stars. Our main source was the catalog of [Fe/H] determination of Cayrel de Strobel et al. (1997), which contains all metallicity estimates in the literature up to 1995. Naturally, this is an inhomogeneous compilation. In an effort

TABLE 3
ADOPTED PHOTOSPHERIC PARAMETERS OF THE STARS

STELLAR ID						PHOTOSPHERIC PARAMETERS			
HR (1)	HD (2)	SAO (3)	BD (4)	Other (5)	SPECTRAL CLASS (6)	$T_{\rm eff}$ (7)	log g (8)	[Fe/H] (9)	Method (10)
				Supergiants					
	104452	82106	22 2430	1 Com	G0 II(32)	−1	99.99	0.00(1)	—
7063.....	173764	142618	−4 4582	β Sct	G4 IIa(32)	4700(2)	0.94(2)	−0.15(2)	s
7314.....	180809	68065	37 3398	θ Lyr	K0 II(32)	4550(2)	1.77(2)	0.14(2)	s
6713.....	164349	103285	16 3335	93 Her	K0.5 II(32)	4383(2)	1.80(2)	−0.22(2)	s
	193515	69825	37 3882	PPM 84702	K1 II(33)	−1	99.99	0.00(1)	—
8465.....	210745	34137	57 2475	ζ Cep	K1.5 Ib(32)	4159(2)	0.88(2)	0.25(2)	s
7735.....	192577	32042	52 2547	o01 Cyg	K2 Ib(34)	4030(5)	1.39(5)	−0.36(5)	s
	192041	69578	38 3939	PPM 84402	K2 II(33)	−1	99.99	0.00(1)	—
6498.....	157999	122387	4 3422	σ Oph	K2 II(32)	−1	99.99	0.01(30)	s
	232078	105082	16 3924	V339 Sge	K3 II(35)	4000(7)	0.40(7)	−1.60(7)	s

NOTES.—Table 3 is available in its entirety in the electronic edition of the *Astrophysical Journal Supplement*. A portion is shown here for guidance regarding its form and content. (Cols. [1]–[5]) Stellar identifiers: HR, HD, SAO, BD, etc. Abreviations: B = Blanco (1986), BMB = Blanco et al. (1984), and TLE = Lloyd Evans (1976). For more details see Worthey et al. (1994). (Col. [6]) Spectral classification; The number in parentheses is the reference source. (Cols. [7]–[9]) Photosperic parameters: effective temperature $T_{\rm eff}$, surface gravity log g, abundance [Fe/H]. Unknown entries have values −1 for $T_{\rm eff}$, and 99.99 for log g and [Fe/H]. The number in parentheses is the reference source. (Col. [10]) Method used to estimate the abundance: s, spectroscopy; b, broadband photometry; n, narrowband photometry; a dash indicates none—the value is unknown or assumed.

REFERENCES.—(1) Tentatively assumed solar abundance for the supergiants and [Fe/H] $= -0.21$ for the bulge giants (Ramírez et al. 2000b); (2) Cayrel de Strobel et al. 2001 and references therein; (3) Gorgas et al. 1993 and references therein; (4) van Dyck et al. 1998; (5) Taylor 1999 and references therein; (6) Zhou Xu 1991; (7) Worthey et al. 1994 and references therein; (8) Faber et al. 1985 and references therein; (9) Di Benedetto 1998; (10) Santos et al. 2003; (11) Garmany & Stencel 1992; (12) Lee 1970; (13) Luck & Bond 1989; (14) Feltzing & Gustafsson 1998; (15) Taylor et al. 1972; (16) Alonso et al. 1994; (17) Bell & Gustafsson 1989; (18) Eggen 1998; (19) Dumm & Schild 1998; (20) van Belle et al. 1999; (21) Taylor 1991; (22) Eggen 1996; (23) Zakhozhaj & Shaparenko 1996; (24) Kirkpatrick et al. 1993; (25) Leggett et al. 1996; (26) Leggett et al. 2000; (27) Bidelman 1957; (28) Johnson 1966; (29) Ramírez et al. 2000a; (30) Cayrel de Strobel et al. 1997 and references therein; (31) Lloyd Evans 1976; (32) Keenan & McNeil 1989; (33) Barbier 1962; (34) Ginestet & Carquillat 2002; (35) Preston & Bidelman 1956; (36) Houk & Smith-Moore 1988; (37) Humphreys 1970; (38) Sloan & Price 1998; (39) Cowley 1972; (40) Gray et al. 2001; (41) Roman 1952; (42) Keenan & Keller 1953; (43) Greenstein & Keenan 1958; (44) Upgren & Staron 1970; (45) Fernie 1959; (46) Fehrenbach et al. 1962; (47) Schmitt 1971; (48) Roman 1955; (49) Halliday 1955; (50) Eaton 1995; (51) Eggen & Stokes 1970; (52) Appenzeller 1967; (53) Johnson & Morgan 1953; (54) Cowley et al. 1969; (55) Lutz & Lutz 1977; (56) Morgan et al. 1953; (57) Haywood 2001; (58) Abt 1981; (59) Harlan 1969; (60) Barbier 1968; (61) Nassau & van Algabada 1947; (62) Henry et al. 1994; (63) Joy & Abt 1974; (64) Kirkpatrick et al. 1991; (65) Blanco et al. 1984; (66) Blanco 1986; (67) Brown et al. 1989.

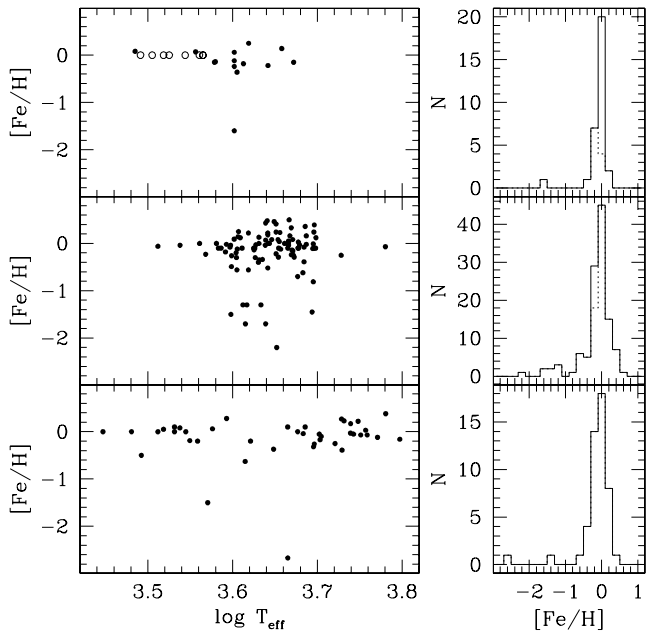

FIG. 7.—Metallicity of library stars [Fe/H] vs. the effective temperature $T_{\rm eff}$ (*left panels*), and metallicity histograms (*right*) for supergiants, giants, and dwarfs (*from top to bottom*). The stars with parameters adopted from the literature are shown with solid dots, and the stars with assumed parameters are circles. Solid-line histograms include all stars with adopted or assumed metallicity, and dotted-line histograms omit the assumed values.

to "homogenize" the data as much as possible—at least in terms of abundance estimate methods—we used spectroscopic determinations when possible. Only did we use metallicities based on narrowband photometry when these were the only estimates available in the literature. Broadband photometry based metallicities were adopted for six dwarf stars with no other measurements.

We made some assumptions when no photospheric parameters could be found in the literature: (*i*) solar metallicity was adopted for supergiants in the Galactic disk, and (*ii*) [Fe/H] $= -0.21$ was adopted for all bulge stars, following (Ramírez et al. 2000b). We neglect the 0.3 dex of metallicity dispersion in the bulge, until individual estimates become available. We included in the table some color information—the reddening corrected $(V-K)_0$—for stars with unknown spectral class.

The metallicities as a function of the luminosity class for stars in our library are shown in Figure 7. The giants show the largest [Fe/H] spread by far. The supergiants suffer from a pure astrophysical constraint: the massive metal-poor stars from Population II (and possibly III) in our Galaxy exploded as supernovae a long time ago. The Magellanic Clouds offer a possibility to complement the library with some supergiants with 1/5 to 1/20 of the solar metallicity (Luck et al. 1998; Hill 1999). Obtaining such spectra is foreseen in the next papers of this series.

4. INDEX DEFINITIONS

Some spectral features in the near-IR have been observed and measured, and suitable spectral indices have already been defined by Kleinmann & Hall (1986), Origlia et al. (1993), Doyon, Joseph, & Wright (1994), and Ali et al. (1995). We adopted their definitions for compatibility, with two modifications. First, for the Na I and Ca I indices of Ali et al. (1995) we used only the two nearest continuum bands. Second, for the CO index of Doyon et al. (1994) we carried a polynomial, rather than a power-law, fit to the continuum. Experiments show that both these changes produce no significant effects, within the errors.

Our spectra do not always span the wavelength range of the original photometric CO index of Frogel et al. (1978), and we were forced to measure only narrow spectral indices, including the one defined by Ivanov et al. (2000). The latter is somewhat intermediate between the narrow and broad CO

TABLE 4
DEFINITIONS OF SPECTRAL BANDS

		LINE[a]		CONT. 1[a]		CONT. 2[a]		
NO.	SPECIES	λ_c (Å)	$\Delta\lambda$ (Å)	λ_c (Å)	$\Delta\lambda$ (Å)	λ_c (Å)	$\Delta\lambda$ (Å)	REFERENCE
1.....	Mg I (1.50 μm)	15040	40	15005	30	15075	30	1
2.....	Fe I (1.58 μm)	15830	40	15800	20	15857.5	15	1
3.....	Si I (1.59 μm)	15890	40	15850	40	15930	40	3
4.....	CO (1.62 μm)	16197.5	45	16160	30	16270	30	3
5.....	Mg I (1.71 μm)	17115	30	17092.5	15	17145	30	1
6.....	Mg I (2.11 μm)	21075	70	21020	40	21130	40	1
7.....	Brγ (2.16 μm)	21662.5	47	20929	44	22899	52	2
8.....	Na I (2.21 μm)	22075	70	22170	60	22350	40	4
9.....	Na I (2.21 μm)	22077	48	20929	44	22899	52	2
10.....	Ca I (2.26 μm)	22635	110	22510	40	22720	40	4
11.....	Ca I (2.26 μm)	22636.5	51	20929	44	22899	52	2
12.....	Mg I (2.28 μm)	22806	52	22750	60	22857	50	1
13.....	Mg I (2.28 μm)	22820	60	22720	40	22886	30	4
14.....	CO (2.29 μm)	22950.5	53	22899	52			3
15.....	^{12}CO (2, 0) (2.29 μm)	22957	52	22899	52			2
16.....	CO (2.29 μm)	22980	100	22850	100			6
17.....	^{12}CO (3, 1) (2.32 μm)	23245	54	22899	52			2
18.....	^{13}CO (2, 0) (2.35 μm)	23463.5	55	22899	52			2
19.....	CO (2.35 μm)	23550	900					5

[a] Central wavelength λ_c and bandwidth $\Delta\lambda$, in Å.

REFERENCES.—(1) This work; (2) Kleinmann & Hall 1986; (3) Origlia et al. 1993; (4) Ali et al. 1995; (5) Doyon et al. 1994; (6) Ivanov et al. 2000.

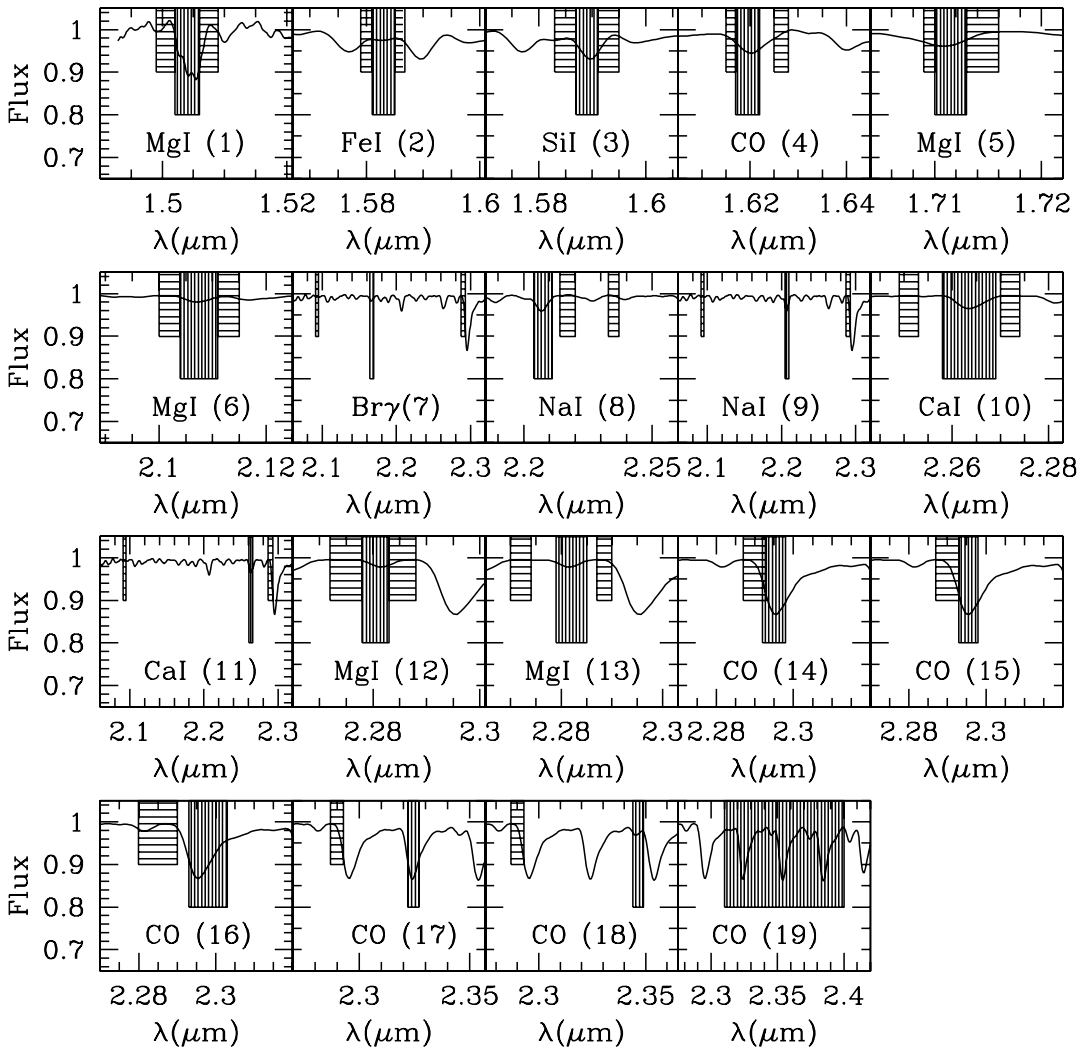

FIG. 8.—Definitions of the spectral indices. The vertically shaded area represents the line band, and the horizontally shaded areas are the continuum bands. Note that the last index is measured after the continuum normalization over the entire K spectra and has no proper continuum band. The numbers in parentheses in each panel correspond to the index numbering in Table 4.

TABLE 5

SPECTRAL INDICES OF FEATURES OF INTEREST

Star ID	Mg (1)	Fe (2)	Si (3)	CO (4)	Mg (5)	Mg (6)	Brγ_k (7)	Na (8)	Na (9)	Ca (10)	Ca (11)	Mg (12)	Mg (13)	CO (14)	CO (15)	CO (16)	CO (17)	CO (18)	CO (19)
Supergiants																			
SAO 082106.....	0.04	0.01	0.04	0.01	0.00	0.00	0.08	0.01	0.01	0.01	0.00	0.01	0.02	0.02	0.02	0.01	0.01	0.01	0.01
HR 7063.....	0.06	0.04	0.07	0.03	0.02	0.01	0.07	0.00	0.03	0.01	0.03	0.01	0.01	0.16	0.15	0.09	0.14	0.01	0.05
HR 7314.....	0.08	0.03	0.03	0.06	0.03	0.02	0.01	0.03	0.03	0.04	0.05	0.00	0.01	0.06	0.10	0.11	0.20	0.02	0.07
HR 6713.....	0.07	0.03	0.10	0.05	0.03	0.02	0.04	0.00	0.04	0.01	0.02	0.02	0.02	0.22	0.23	0.14	0.19	0.01	0.06
SAO 069825.....	0.07	0.02	0.02	0.02	0.03	0.02	0.07	0.02	0.02	0.02	0.02	0.01	0.01	0.03	0.05	0.06	0.12	0.00	0.04
HR 8465.....	0.10	0.04	0.10	0.11	0.03	0.01	0.03	0.03	0.06	0.01	0.04	0.02	0.01	0.36	0.38	0.25	0.31	0.07	0.09
HR 7735.....					0.04														
SAO 069578.....	0.11	0.03	0.04	0.07	0.04	0.01	0.03	0.04	0.06	0.03	0.05	0.01	0.01	0.06	0.10	0.12	0.24	0.06	0.08
HR 6498.....	0.10	0.02	0.08	0.11	0.03	−0.01	0.00	0.03	0.03	0.00	0.02	0.00	−0.01	0.34	0.34	0.26	0.20	0.02	0.08
SAO 105082.....	0.02	−0.01	0.07	0.04	−0.06	0.01	−0.04	0.00	−0.07	0.00	−0.11	0.00	−0.01	0.03	0.01	0.09	−0.02	−0.09	0.05

NOTES.—Table 5 is available in its entirety in the electronic edition of the *Astrophysical Journal Supplement*. A portion is shown here for guidance regarding its form and content. Indices are given in magnitudes. The numbers in the heading correspond to the numbers of index definitions given in Table 4. Stars are sorted in order of luminosity and spectral class, same as in Table 3.

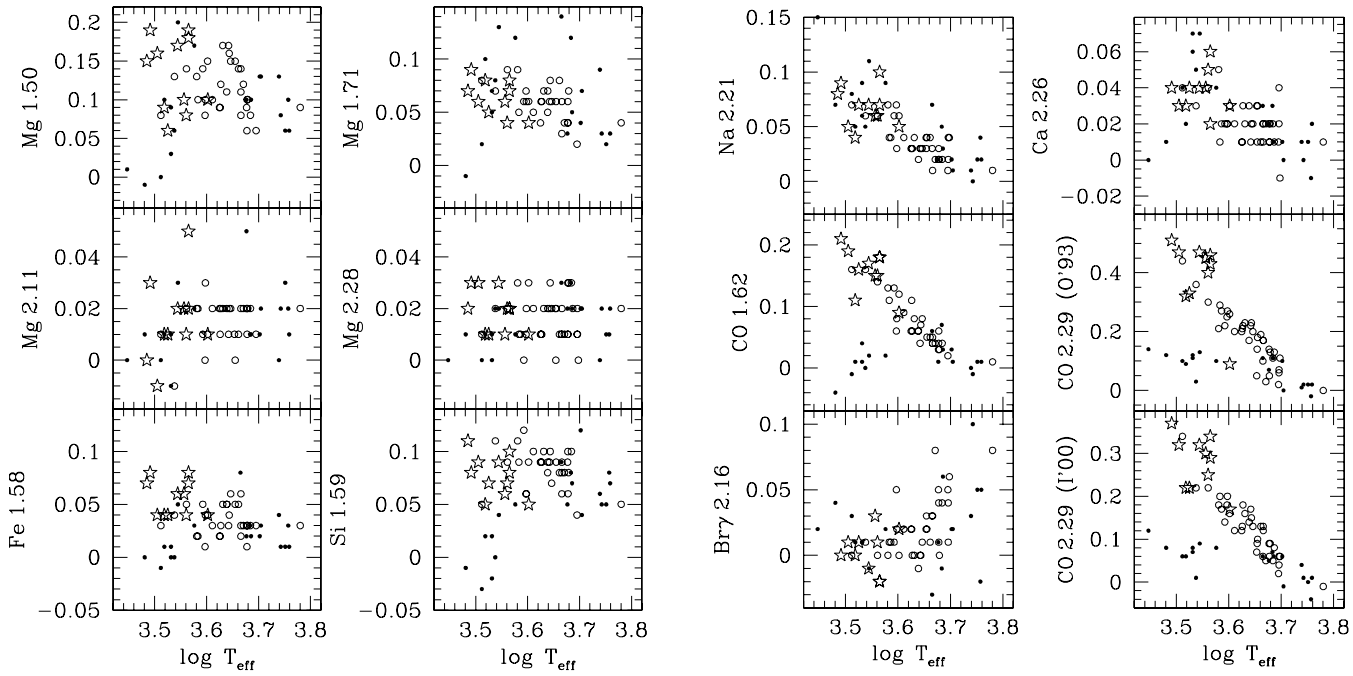

FIG. 9.—Line indices as temperature indicators. The Si and the CO (*upper panel*) definitions are from Origlia et al. (1993), the Brγ is from Kleinmann & Hall (1986), the CO (*lower panel*) is from Ivanov et al. (2000), and all Mg I and Fe indices are from this work. Star symbols indicate supergiants, open circles are giants, and solid dots represent dwarfs and subgiants. All indices are in magnitudes. The typical measurement error is $\sigma = 0.02$ mag. Only stars with $-0.10 \leq [\mathrm{Fe/H}] \leq +0.10$ are shown.

indices, which makes it less sensitive to variations of the photospheric transmission. It provides better signal-to-noise ratio than the narrower spectroscopic indices.

Finally, we defined new indices for atomic lines that had not been measured before, or where the previous definitions could be affected by the loss of the true continuum shape as discussed above, for instance, the indices defined by Kleinmann & Hall (1986), where the continuum bands are very far apart. All definitions are summarized in Table 4, and the bandpasses are shown in Figure 8. The measured indices for the library stars are given in Table 5. The gaps in the table are due to incomplete spectral coverage.

All indices are in magnitudes:

$$\mathrm{Index} = -2.5 \times \log_{10}(I_{\mathrm{line}}/I_{\mathrm{continuum}}), \qquad (1)$$

where I_{line} is the flux in the line band, normalized by the bandwidth, and $I_{\mathrm{continuum}}$ is linear interpolation of the continuum flux at the line wavelength. An exception are the CO bands for which $I_{\mathrm{continuum}}$ is the bandwidth normalized flux in the continuum pass band.

5. DIAGNOSTICS OF INDIVIDUAL STARS

5.1. *Stellar Effective Temperature Indicators*

Many near-IR spectral features are good indicators of the stellar effective temperature (T_{eff}) by themselves, e.g., the CO bands, and the Na I, Ca I indices (Kleinmann & Hall 1986). Figure 9 shows the behavior of all measured features as function of T_{eff}. To minimize metallicity effects we only plot stars with $-0.10 \leq [\mathrm{Fe/H}] \leq +0.10$. The CO bands, Brγ, Na, and Ca show stronger temperature dependence than, for instance, Mg, Fe, and Si. This behavior has been demonstrated before (Kleinmann & Hall 1986; Ali et al. 1995; Förster-Schreiber 2000).

Some line ratios, for instance, EW(CO 1.62)/EW(Si I 1.59) (Origlia et al. 1993; Dallier, Boisson, & Joly 1996; Förster-Schreiber 2000), are better temperature indicators than individual lines because the division cancels out any additional luminosity, metallicity, or reddening effects. Based on the indices

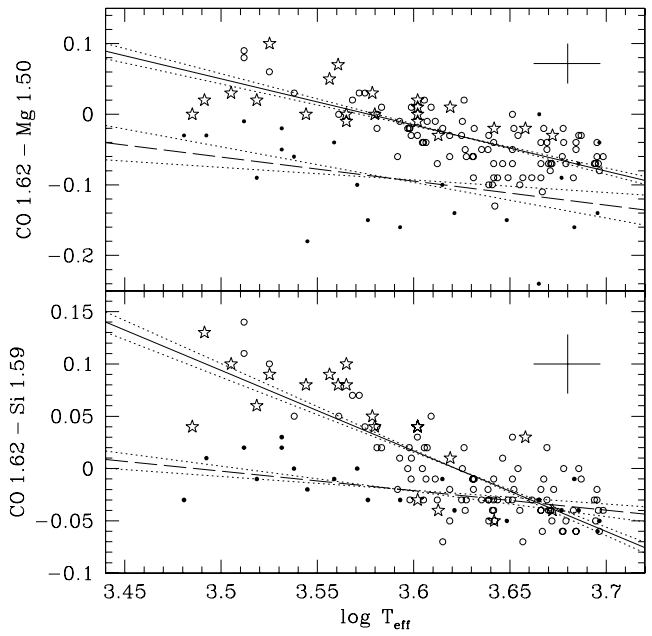

FIG. 10.—Line ratios as temperature indicators. The CO and Si I definitions are from Origlia et al. (1993), and the Mg I is from this work. All indices are in magnitudes. Star symbols indicate supergiants, open circles are giants, and solid dots represent dwarfs and subgiants. The typical ± 1 σ measurement error is shown in the top right corner. The best linear fits to supergiants and giant are shown with a solid line, and the best fit to dwarfs and subgiants is a dashed line. The dotted lines represent ± 1 σ errors in the slopes.

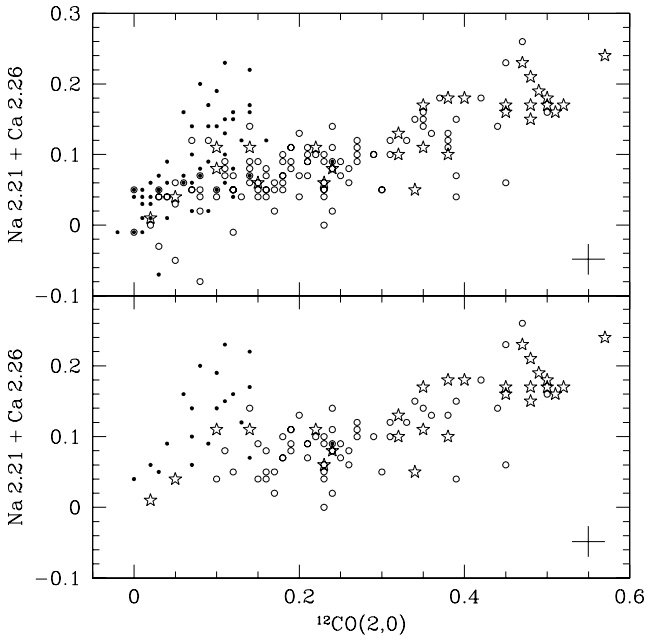

FIG. 11.—Two-dimensional spectral classification. Comparison of the strengths of Na and Ca features, with the 2.29 μm CO bandhead absorption, following Kleinmann & Hall (1986). All index definitions are from there, and the indices are in magnitudes. Star symbols indicate supergiants, open circles are giants, and solid dots represent dwarfs and subgiants. The typical ± 1 σ observational uncertainties are shown in the bottom right corner. The top panel includes all stars, the bottom panel shows only stars with [Fe/H] ≥ -0.5 and $T_{\rm eff} \leq 4500$ K.

of 109 stars from our sample (Fig. 10), we find the following relation for giants and supergiants with $T_{\rm eff} \leq 5000$ K:

$$(\mathrm{CO\ 1.62} - \mathrm{Si\ I\ 1.59}) = (2.79 \pm 0.19) - (0.77 \pm 0.05) \times \log T_{\rm eff}. \quad (2)$$

Here we used the index definitions of Origlia et al. (1993). The root mean square (rms) of the relation is 0.03 mag, which corresponds to $\sim$300 K for the inverse equation, close to the typical observational errors of 0.02 mag. From indices of 23 dwarfs and subgiants, again with $T_{\rm eff} \leq 5000$ K:

$$(\mathrm{CO\ 1.62} - \mathrm{Si\ I\ 1.59}) = (0.65 \pm 0.20) - (0.19 \pm 0.05) \times \log T_{\rm eff}, \quad (3)$$

where the rms is 0.02 mag, corresponding to $\sim$800 K. The slopes of the relations are significantly different, and the loci of the two groups overlap only for hot stars where both spectral features are weak and the relative errors increase.

We derived similar relations using the 1.50 μm Mg I feature. For 107 giants and supergiants:

$$(\mathrm{CO\ 1.62} - \mathrm{Mg\ I\ 1.50}) = (2.34 \pm 0.21) - (0.65 \pm 0.06) \times \log T_{\rm eff}. \quad (4)$$

The CO index is defined by Origlia et al. (1993), and the Mg I index is defined in this work. The rms is 0.03 mag or $\sim$350 K. For 23 dwarfs and subgiants:

$$(\mathrm{CO\ 1.62} - \mathrm{Mg\ I\ 1.50}) = (1.13 \pm 0.59) - (0.34 \pm 0.16) \times \log T_{\rm eff}, \quad (5)$$

with rms of 0.06 mag or $\sim$1500 K. The relations for dwarfs and subgiants are worse than for giants and supergiants because of both weaker spectral lines and systematically fainter targets. Note that even though we have not restricted the abundances, the majority of stars used to derive the equations above have near-solar metallicities ($-0.2 \leq$ [Fe/H] $\leq +0.2$) and abundance ratios.

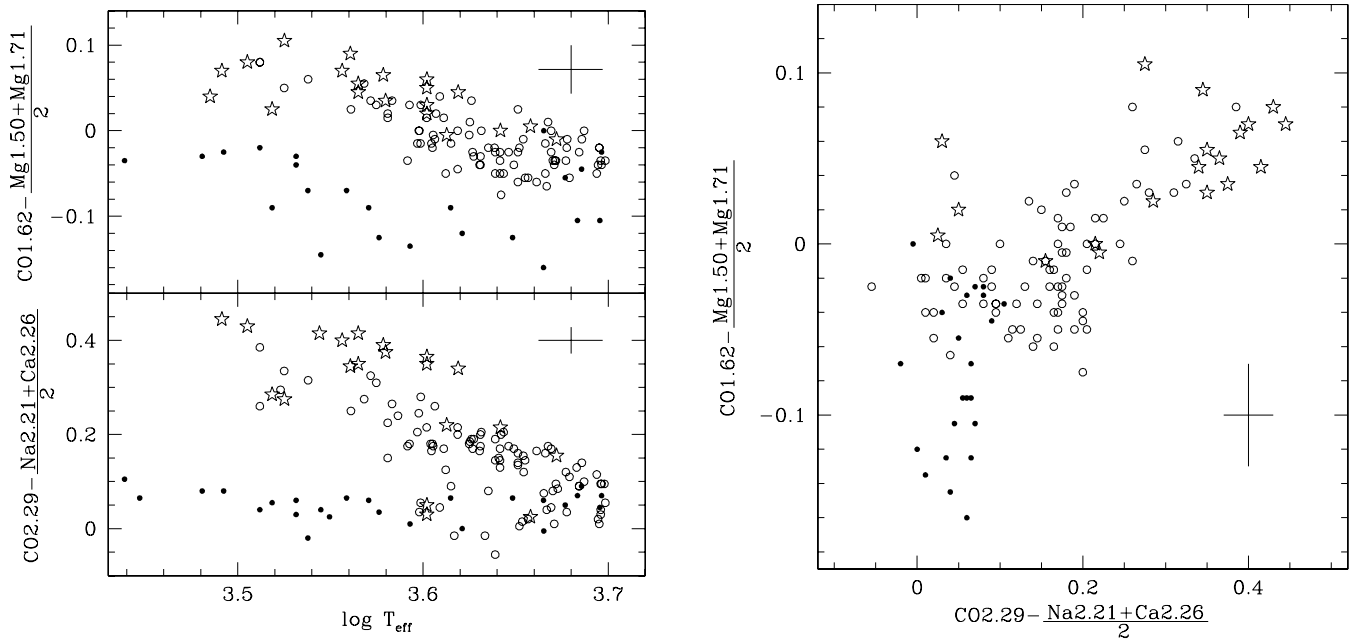

FIG. 12.—Two-dimensional spectral classification with *H*-band features (*top left*) and *K*-band features (*bottom left*), and their combination (*right*). All indices are in magnitudes. The stellar effective temperature $T_{\rm eff}$ is used on the left plot, and only pure observables are used on the right. Star symbols indicate supergiants, open circles are giants, and solid dots represent dwarfs and subgiants. The typical ± 1 σ measurement error is shown in the bottom right corner. The CO bands are defined by Origlia et al. (1993), the Ca and Na indices are from Ali et al. (1995), and the Mg definitions are from this work.

5.2. *Two-dimensional Spectral Classification—Luminosity Class Indicators*

The two-dimensional spectral classification requires an indicator for the intrinsic luminosity of the stars. Kleinmann & Hall (1986) demonstrated that Na, Ca, and Brγ can be used to discriminate between stars of different luminosity classes (see their Fig. 7). We verified their result, excluding the Brγ index (Fig. 11) to minimize the uncertainties related to the removal of the intrinsic Brγ absorption in the telluric standards (§ 3). The (super)giant versus dwarf separation is relatively small, compared with the typical observational uncertainties. The situation improves if we constrain the sample only to metal-rich stars with [Fe/H] ≥ -0.5 (*bottom panel*), minimizing the relative errors. Clearly, this diagnostic relationship imposes a high demand on the data quality.

Ramírez et al. (1997) proposed to use the log {EW(CO 2.29)/[EW(Na I 2.21) + EW(Ca I 2.26)]} ratio plotted against $T_{\rm eff}$ to separate giants from dwarfs (see their Fig. 11). Our data confirm this result (Fig. 12, *bottom left*), even for higher $T_{\rm eff}$-values than Ramírez et al. (1997) because of the improved S/N and spectral resolution. We obtain similar separation with Mg features (Fig. 12, *top left*). This methods use a physical quantity—$T_{\rm eff}$—that requires some calibration to be derived from observables such as $(V-K)_0$ or some spectral feature. To avoid this additional step, we combined the two ratios—log {EW(CO 2.29)/[EW(Na I 2.21) + EW(Ca I 2.26)]} and log {EW(CO 1.62)/[EW(Mg I 1.50) + EW(Mg I 1.71)]}—and found that we can still achieve separation for most of the stars.

The signal-to-noise ratio needed to use the diagnostics discussed here depends on the temperature of the stars. It is safe to assume that S/N $\sim$ 30 is necessary for K5–M stars, and it increases up to 50 for early K stars. The lines become too weak to implement these techniques for stars with effective temperatures hotter than 4500–4800 K. An additional limitation comes from the metal abundance—it is more difficult to separate stars of different luminosity class with low metallicity than with high metallicity, because in the former the lined are weaker, and the relative uncertainties are higher. However, our library does not offer sufficient abundance range to quantify this effect.

6. SUMMARY

We have assembled a library of moderately high-resolution ($\approx$2000–3000) H (1.6 μm) and K (2.2 μm) spectra of 218 red stars, mostly supergiants and giants. The majority of these stars have well-known photospheric parameters from high-resolution optical spectroscopy. These stars dominate the near-IR emission in both starburst and elliptical galaxies. Our library covers a range of effective temperatures, and metal abundances from [Fe/H] ~ -2.2 to +0.3. This library will offer a unique opportunity to study directly the most obscured stellar populations in starburst galaxies, as well as in the center of the Milky Way.

Although the main motivation behind the creation of this library is the study of unresolved extragalactic stellar populations, the obtained spectra can be used to derive parameters of individual stars. We calibrated some line ratios as indicators of the stellar effective temperature. Finally, we demonstrated how some diagnostic relationships can distinguish (super)-giants from dwarf stars.

This research has made use of the SIMBAD database, operated at CDS, Strasbourg, France. The authors were supported by NSF grant AST 95-29190. We are grateful to the anonymous referee for the suggestions that helped to improve the paper.

REFERENCES

Abt, H. A. 1981, ApJS, 45, 437
Ali, B., Carr, J. S., Depoy, D. L., Frogel, J. A., & Sellgren, K. 1995, AJ, 110, 2415
Aloisi, A., Savaglio, S., Heckman, T. M., Hoopes, C. G., Leitherer, C., & Sembach, K. R. 2003, ApJ, 595, 760
Alonso, A., Arribas, S., & Martinez-Roger, C. 1994, A&AS, 107, 365
Appenzeller, I. 1967, PASP, 79, 102
Barbier, M. 1962, J. des Obs., 45, 57
———. 1968, Publ. Obs. Haute-Provence, 9, 38
Bell, R. A., & Gustafsson, B. 1989, MNRAS, 236, 653
Bidelman, W. P. 1957, PASP, 69, 326
Blanco, V. M. 1986, AJ, 91, 290
Blanco, V. M., McCarthy, M. F., & Blanco, B. M. 1984, AJ, 89, 636
Brown, J. A., Sneden, C., Lambert, D. L., & Dutchover, E., Jr. 1989, ApJS, 71, 293
Bruzual, G. A., & Charlot, S. 1993, ApJ, 405, 538
Casuso, E., Vazdekis, A., Peletier, R. F., & Beckman, J. E. 1996, ApJ, 458, 533
Cayrel de Strobel, G., Soubiran, C., Friel, E. D., Ralite, N., & François, P. 1997, A&AS, 124, 299
Cayrel de Strobel, G., Soubiran, C., & Ralite, N. 2001, A&A, 373, 159
Cowley, A. 1972, AJ, 77, 750
Cowley, A., Cowley, C., Jaschek, M., & Jaschek, C. 1969, AJ, 74, 375
Dallier, R., Boisson, C., & Joly, M. 1996, A&AS, 116, 239
Di Benedetto, G. P. 1998, A&A, 339, 858
Doyon, R., Joseph, R. D., & Wright, G. S. 1994, ApJ, 421, 101
Dumm, T., & Schild, H. 1998, NewA, 3, 137
Eaton, J. A. 1995, AJ, 109, 1797
Eggen, O. J. 1996, AJ, 111, 466
———. 1998, AJ, 115, 2397
Eggen, O. J., & Stokes, N. R. 1970, ApJ, 161, 199
Engelbracht, C. W. 1997, Ph.D. thesis, Univ. Arizona
Faber, S. M., Friel, E. D., Burstein, D., & Gaskell, C. M. 1985, ApJS, 57, 711
Fehrenbach, C., Rebeirot, E., Petit, M., Peyrin, Y., & Monvoisin, C. 1962, J. des Obs., 45, 349
Feltzing, S., & Gustafsson, B. 1998, A&A, 129, 237
Fernie, J. D. 1959, ApJ, 130, 610
Förster-Schreiber, N. M. 2000, AJ, 120, 2089
Frogel, J. A., Persson, S. E., Aaronson, M., & Matthews, K. 1978, ApJ, 220, 75
Garmany, C. D., & Stencel, R. E. 1992, A&AS, 94, 211
Ginestet, N., & Carquillat, J. M. 2002, ApJS, 143, 513
Gorgas, J., Faber, S. M., Burstein, D., Gonzalez, J. J., Courteau, S., & Prosser, C. 1993, ApJ, 86, 153
Gray, R. O., Napier, M. C., & Winkler, L. I. 2001, AJ, 121, 2148
Greenstein, J. L., & Keenan, P. C. 1958, ApJ, 127, 172
Halliday, I. 1955, ApJ, 122, 222
Hanson, M. M., Conti, P. S., & Rieke, M. J. 1996, ApJS, 107, 281
Harlan, E. A. 1969, AJ, 74, 916
Haywood, M. 2001, MNRAS, 325, 1365
Henry, T. J., Kirkpatrick, J. D., & Simons, D. A. 1994, AJ, 108, 1437
Hicks, E. K., Malkan, M. A., Teplitz, H. I., Sugai, H., & Guichard, J. 2000, BAAS, 197, 4408
Hill, V. 1999, A&A, 345, 430
Houk, N., & Smith-Moore, M. 1988, Michigan Spectral Survey (Ann Arbor: Univ. Michigan), 4
Humphreys, R. M. 1970, AJ, 75, 602
Ivanov, V. D., Rieke, G. H., Groppi, C. E., Alonso-Herrero, A., Rieke, M. J., & Engelbracht, C. W. 2000, ApJ, 545, 190
Johnson, H. L. 1966, ARA&A, 4, 193
Johnson, H. J., & Mèndez, M. E. 1970, AJ, 75, 785
Johnson, H. J., & Morgan, W. W. 1953, ApJ, 117, 313
Joy, A. H., & Abt, H. A. 1974, ApJS, 28, 1
Joyce, R. R. 1998, AJ, 115, 2059
Keenan, P. C., & Keller, G. 1953, ApJ, 117, 241
Keenan, P. C., & McNeil, R. C. 1989, ApJS, 71, 245

Kirkpatrick, J. D., Henry, T. J., & McCarthy, D. W., Jr. 1991, ApJS, 77, 417
Kirkpatrick, J. D., Kelly, D. M., Rieke, G. H., Liebert, J., Allard, F., & Wehrse, R. 1993, ApJ, 402, 643
Kleinmann, S. G., & Hall, D. N. B. 1986, ApJS, 62, 501
Kozlowski, L. J., Kadri, V., Cooper, D. E., Bailey, R. B., Bui, D. Q., & Stephenson, D. M. 1993, Proc. SPIE, 1946, 149
Kurucz, R. 1994, Kurucz CD-ROM 19 (Cambridge: SAO)
Lançon, A., & Rocca-Volmerange, B. 1992, A&AS, 96, 593
Lançon, A., & Wood, P. R. 2000, A&AS, 146, 217
Lee, T. A. 1970, ApJ, 162, 217
Leggett, S. K., Allard, F., Berriman, G., Dahn, C. C., & Hauschildt, P. H. 1996, ApJS, 104, 117
Leggett, S. K., Allard, F., Dahn. C., Hauschildt, P. H., Kerr, T. H., & Rayner, J. 2000, ApJ, 535, 965
Leitherer, C., et al. 1999, ApJS, 123, 3
Livingston, W., & Wallace, L. 1991, An Atlas of the Solar Spectrum in the Infrared from 1850 to 9000 cm^{-1} (1.1 to 5.4 μm), NSO, Tech. Rep. 91-001 (Tucson: NSO)
Lloyd Evans, T. 1976, MNRAS, 174, 169
Luck, R. E., & Bond, H. E. 1989, ApJS, 71, 559
Luck, R. E., Moffet, T. J., Barnes III, T. G., & Gieren, W. P. 1998, AJ, 115, 605
Lutz, T. E., & Lutz, J. H. 1977, AJ, 82, 431
Maiolino, R., Rieke, G. H., & Rieke, M. J. 1996, AJ, 111, 537
McWilliam, A., & Rich, R. M. 1994, ApJS, 91, 749
Merrill, K. M., & Ridgway, S. T. 1979, ARA&A, 17, 9
Meyer, M. R., Edwards, S., Hinkle, K. H., & Strom, S. E. 1998, ApJ, 508, 397
Morgan, W. W., Harris, D. L., & Johnson, H. L. 1953, ApJ, 118, 92
Nassau, J. J., & van Algabada, G. B. 1947, ApJ, 106, 20
Oliva, E., & Origlia, L. 1992, A&A, 254, 466
Origlia, L., Moorwood, A. F. M., & Oliva, E. 1993, A&A, 280, 536
Preston, G. W., & Bidelman, W. P. 1956, PASP, 68, 533
Ramírez, S. V., DePoy, D. L., Frogel, J. A., Sellgren, K., & Blum, R. D. 1997, AJ, 113, 1411
Ramírez, S. V., Sellgren, K., Carr, J. S., Balachandran, S. C., Blum, R., Terndrup, D. M., & Steed, A. 2000a, ApJ, 537, 205
Ramírez, S. V., Stephens, A. W., Frogel, J. A., & DePoy, D. L. 2000b, AJ, 120, 833
Rieke, G. H., & Lebofsky, M. J. 1985, ApJ, 288, 618
Rieke, G. H., Lebofsky, M. J., Thompson, R. I., Low, F. J., & Tokunaga, A. T. 1980, ApJ, 238, 24
Rieke, G. H., Locken, K., Rieke, M. J., & Tamblyn, P. 1993, ApJ, 412, 99
Roman, N. G. 1952, ApJ, 116, 122
———. 1955, ApJS, 2, 195
Santos, N. C., Israelian, G., Mayor, M., Rebolo, R., & Udry, S. 2003, A&A, 398, 363
Schmidt-Kaler, T. 1982, in Landolt-Borstein, New Series, Group VI, vol. 2, ed. K. Schaifers & H. H. Voigt (Berlin: Springer), 1
Schmitt, J. L. 1971, ApJ, 163, 75
Sloan, G. C., & Price, S. D. 1998, ApJS, 119, 141
Straižys, V. 1992, Multicolor Stellar Photometry (Tucson: Pachart Pub.)
Taylor, B. J. 1991, ApJS, 76, 715
———. 1999, A&A, 134, 523
Taylor, B. J., Spinrad, H., & Schweizer, F. 1972, ApJ, 173, 619
Upgren, A. R., & Staron, R. T. 1970, ApJS, 19, 367
van Belle, G. T., et al. 1999, AJ, 117, 521
van Dyck, H. M., van Belle, G. T., & Thompson, R. R. 1998, AJ, 116, 981
Vazdekis, A. 1999, ApJ, 513, 224
Wallace, L., & Hinkle, K. 1996, ApJS, 107, 312
———. 1997, ApJS, 111, 445
Wallace, L., Meyer, M. P., Hinkle, K., & Edwards, S. 2000, ApJ, 535, 325
White, N. M., & Wing, R. F. 1978, ApJ, 222, 209
Williams, D. M., Thompson, C. L., Rieke, G. H., & Montgomery, E. F. 1993, Proc. SPIE, 1946, 482
Worthey, G. 1994, ApJS, 95, 107
Worthey, G., Faber, S. M., Gonzalez, J. J., & Burstein, D. 1994, ApJS, 94, 687
Zakhozhaj, V. A., & Shaparenko, E. F. 1996, Kin. Fiz. Nebesn. Tel., 12, 20
Zhou Xu. 1991, A&A, 248, 367